Kinetic Studies of $LaCoO_{3-\delta}$ Preparation from Solid State Reactions

Baijun Yan, Jiayun Zhang and Jianhua Liu

Department of Physical Chemistry, University of Science and Technology Beijing Beijing 100083, China

(Received March 1, 2004; final form March 23, 2004)

ABSTRACT

The present paper deals with kinetics of $LaCoO_{3-\delta}$ preparation with La_2O_3 and Co_3O_4 powder mixture. High temperature X-ray diffraction measurements were carried out in air, combining with TG-DSC technique, between 298K and 1473K. The results have exhibited the reaction between La_2O_3 and Co_3O_4 starting around 1093K, and no intermediate compound forming between them.

The kinetic study of $LaCoO_{3-\delta}$ preparation was further performed using pressed La_2O_3 and Co_3O_4 powder mixture compacts under isothermal calcinations at several temperatures between 983K and 1223K. Three-dimensional diffusion models have been employed to describe the isothermal synthesis process satisfactorily. The resultant activation energy obtained was 233.6 kJ/mol in average. Lanthanum ion diffusion in the product layer could be the rate-controlling step of the overall process.

1. INTRODUCTION

There has been a growing interest in perovskites of composite compounds between rare earth and transition metal oxides since the middle of 1980s /1-19/. The reason has been due to their specific catalytic, oxygen permeation properties, as well as the high electric and ionic conductivities. Lanthanum cobaltate, $LaCoO_{3-\delta}$, has a perovskite structure with rhombohedral distortion, exhibiting attractive electrical and magnetic properties due to the coexistence of low- and high-spin cobalt ions in it /4/. A-site or/and B-site doping to lanthanum cobaltate perovskites has been a principle measure influencing the variation of the defect structure, and therefore, their electric, magnetic, catalytic properties. Some of these ceramic materials have been effectively applied to SOFC /9-11, 18/, catalyst in redox reactions at relatively low temperature /12/ and so on /13-15/.

The oxygen nonstoichiometry of a perovskite-type ceramic with respect to oxygen partial pressure and temperature is critical to many applications, such as sorbents in a recently proposed adsorption separation process for air separation or oxygen removal and as membranes for partial oxidation reactions of hydrocarbons. Seppänen /1/ determined the ionic defect structure of a single-phase $LaCoO_{3-\delta}$, as well as $LaCoO_{3-\delta}$ in equilibrium with CoO and La_2O_3 in a range from 1178K to 1311K using coulometric titration method, and found δ is almost proportional to $p_{O_2}^{-1/2}$. Mizusaki /20/ determined the oxygen nonstoichiometry of $La_{1-x}Sr_xCoO_{3-\delta}$ (x = 0, 0.1, 0.2, 0.3, 0.5 and 0.7) using thermogravimetric measurements in the oxygen partial pressure range, 1Pa < p_{O_2} < 0.1Mpa, between 573K and 1273K. For $LaCoO_{3-\delta}$, Mizusaki /20/ obtained almost the same result as Seppänen, and found that δ could not be detected below 1073K.

As their attractive prospects in applications revealed, in fundamental research these perovskites have also received close attention. Numerous investigations regarding REMe (Me=Co, Mn, Fe) $O_{3\pm\delta}$ can be found in scientific literature in recent years. The fundamental studies have been mainly concentrated on the structure, properties as well as the relationship between the same

for perovskite materials, involving $LaCoO_{3-\delta}$ /1, 2, 3, 10, 21/ and the lanthanum cobaltates with various A-site or/and B-site dopings /5,8,11,13,14,17,18/.

Regarding the preparation techniques, a variety of synthesis routes using chemical solutions are commonly recognized as effective in producing fine size particles with higher activities. They are of significance for some of the practical applications. However, the technique of solid-state reactions, as a conventional approach in producing oxide ceramics, still holds a prominent position /9, 3, 14, 16,19 /. This is especially true when investigators try to synthesize newer materials /26-30/. This could be due to the easy and effective composition control, as well as simple operations in synthesizing the perovskite powders in large amounts. It has been noted that XRD combining TG-DTA or TG-DSC measurements as a major technique has been applied to investigate the structure of the materials. High temperature XRD as a dynamic approach has been adopted to examine the structure variations during the synthesizing processes /16,17,21/. Understanding the reaction kinetics and the precise mechanism descriptions of solid-state reactions is of great help in fabricating ceramics. However, too few such investigations have been found in the literature for $REMeO_{3\pm\delta}$ perovskites as well as for the doped perovskites.

A series of studies regarding the kinetics of preparation $REMeO_{3\pm\delta}$ and their doped compounds from solid-state reactions has been carried out by the present group. As the first step, the present paper deals with the kinetic aspects of $LaCoO_{3-\delta}$ synthesis. The $LaCoO_{3-\delta}$ preparation from La_2O_3 and Co_3O_4 powder mixture was monitored using high temperature X-ray diffraction measurements combining with TG-DSC technique between 298K and 1473K. Furthermore, $LaCoO_{3-\delta}$ was prepared isothermally using pressed compacts of La_2O_3 and Co_3O_4 powder mixture in air at temperatures, 983K, 1043K, 1103K, 1133K, 1163K and 1223K respectively. Room temperature XRD measurements with the treatment proposed by Chung *et al.* /22/ were used to determine the fractional conversion of the reactants to $LaCoO_{3-\delta}$ for samples with different heating time for each experimental temperature. The experimental data of the fractional conversion versus time were in turn used to fit to kinetic equations. On such a basis, a solid-state ion diffusion controlling mechanism with the apparent activation energy has been determined.

2. EXPERIMENTAL

La_2O_3 (99.9 pct, 3.92 μm) and Co_3O_4 (spectroscopic purity, 2.69 μm) were used as raw materials in the preparation of $LaCoO_{3-\delta}$ by conventional solid-state reaction. Lanthana was preheated in air at 1223K for 4hrs to remove both absorbed and bonded moisture and carbon dioxide, then cooled in a desiccator to ensure that the weighted data had the required precision. La_2O_3 and Co_3O_4 powder with La/Co molar ratio of 1:1.03 were ball-mixed in a polyethylene jar with silica balls for grinding in alcohol solvent for 3.5hrs and dried at 343K – 353K. The mixed powder was used for high temperature X-ray diffraction and TG-DSC measurements. In addition, this powder mixture was compressed into pellets, for isothermal calcinations.

2.1 High temperature X-ray diffraction measurements

High temperature X-ray diffraction measurements were carried out in air with a flow rate of 0.1667cm^3/s (STP) on a M21X-SRA X-ray diffractometer (MAC Science Co.Ltd, Japan, equipped with graphite crystal diffracted-beam monochromator). The accelerating voltage and current were 40 kV and 300 mA respectively. Operating parameters involved were as follows: 0.1°as divergence slit and scatter slit; 0.15 mm as receiving slit; 25°to 45°as the 2θ scanning range; 8°/min and 0.01°as the scanning speed and step width respectively. The sample was heated from 298K to 1273K with a heating rate of 0.3333K/s (20K/min). When the system reached 298K, 423K, 523K, 623K, 723K, 783K, 853K, 913K, 973K, 1033K, 1093K, 1153K, 1213K and 1273K, the temperature scanning was stopped, and the temperature started to maintain constant for 150s for X-ray diffraction measurements scanning from 25°to 45°(2θ).

2.2 TG-DSC

TG-DSC measurements were carried out in a NETASCH STA 409C thermal analyzer with about

20mg La_2O_3 and Co_3O_4 powder mixture between 298K and 1473K at fixed heating rates of 0.1667K/s (10K/min), 0.3333K/s (20K/min) and 0.5K/s (30K/min) respectively. All measurement runs were carried out in air with a flowing rate of 0.3333cm^3/s (STP).

2.3 $LaCoO_{3-\delta}$ preparation under isothermal calcinations using compressed tablets

The previously prepared La_2O_3 and Co_3O_4 powder mixture was pressed into tablets using a steel die with a pressure of 13.8kN/cm^2. Each tablet was 0.6g in weight and 12mm in diameter.

The tablets were isothermally calcinated in a vertical resistance furnace. The temperature was measured using a Pt-Pt10Rh thermocouple in contact with the center of the bottom of the alumina crucible. A SHIMADEN FP21 programmable controller was used to control the furnace temperature. The experiments were carried out in air to form $LaCoO_{3-\delta}$ at 983K, 1043K, 1103K, 1133K, 1163K and 1223K respectively. In order to reduce the heating and cooling periods, the Al_2O_3 crucible with three tablets held inside (not contacted with each other) was quickly lowered at the middle of the even temperature zone when a specified temperature was reached and stable. At each specified temperature, several experimental runs corresponding to different heating periods were taken. The crucible together with the tablets was pulled out immediately after the heating treatment, and then quenched in air.

Quenched samples were ground in an agate mortar to ensure the mean particle diameter less than 10μm. After grinding, the sample powder was used to take room temperature XRD measurements for determining the fractional conversions. A matrix-flushing approach proposed by Chung /22/ was employed in the quantitative XRD analysis for the multi-component samples. To apply such an approach, a carefully chosen matrix-flushing agent (also called internal standard) is needed to mix with the sample powder to form a so-called composite sample in a preliminarily specified mass ratio. So the composite samples, but not the sample powder directly, were used for room temperature XRD measurements.

In the present study, silver powder was chosen as the matrix-flushing agent. The mass ratio of silver to the sample powder was taken as much as one third. The sample powder and silver powder were thoroughly mixed in agate mortar with alcohol solvent as the mixing agent and dried to form the composite sample.

Room temperature X-ray measurements of composite samples were done in the same X-ray diffractometer as mentioned earlier for high temperature measurements using Cu Kα radiation (40kV, 250mA). Other parameters involved the receiving slit, 0.15mm, divergence slit=0.1°, scatter slit = 0.1°, graphite crystal monochromator. Intensities were collected by scanning from 30°to 40°(2θ) with steps of 0.01°and a rate of 1°/min.

The fractional conversion values converted to $LaCoO_{3-\delta}$ were determined using the intensities of (104) and (110) peaks of $LaCoO_{3-\delta}$ and (111) peak of Ag.

3. RESULTS

3.1 High temperature X-ray diffraction measurements

The $LaCoO_{3-\delta}$ formation was *in-situ* investigated using high temperature X-ray diffraction together with TG-DSC measurements, and the reaction sequences were followed continuously. According to the temperatures and compounds existed, the XRD patterns were divided into four groups, and shown in Fig. 1(a) to Fig. 1(d) respectively. For the sake of clarity, the figure numbers with their corresponding heating temperatures and the existing compounds are listed in Table 1.

Table 1
Compounds existing during high XRD temperature XRD experiments

Figure number	Temperature / K	Compounds
Fig. 1(a)	298, 423, 523, 623	$La(OH)_3$, Co_3O_4
Fig. 1(b)	723, 783, 853	LaOOH, Co_3O_4
Fig. 1(c)	913, 973	La_2O_3, Co_3O_4, $La_2O_2CO_3$
Fig. 1(d)	1033, 1093, 1153, 1213, 1273	$LaCoO_{3-\delta}$, La_2O_3, Co_3O_4

It can be seen from Fig. 1 (a) that La $(OH)_3$, not La_2O_3, existing in the sample, indicating that La_2O_3 was almost completely converted into $La(OH)_3$ during the mixture preparation due to the vapor absorption. This also implies that the experiments started with La $(OH)_3$ and Co_3O_4 mixture rather than "La_2O_3 and Co_3O_4 powder mixture". But for convenience, "La_2O_3 and Co_3O_4 powder mixture" as an expression is still used in the context of this paper. It can be found in Fig. 1 that the mixture underwent the following chemical changes: $La(OH)_3$ decomposition into LaOOH between 623K and 723K; from LaOOH to La_2O_3 between 853K—913K and La_2O_3 conversion into $La_2O_2CO_3$ simultaneously; $La_2O_2CO_3$ decomposition into La_2O_3 between 973K and 1033K before $LaCoO_{3-\delta}$ formation.

It can be seen in Fig. 1 (d) that $LaCoO_{3-\delta}$ started to appear at 1093K, and with the rising temperature the diffraction peaks for $LaCoO_{3-\delta}$ becoming sharp and intense, the peaks of La_2O_3 and Co_3O_4 look smooth gradually. It is known from thermodynamics calculation, Co_3O_4 can be converted into CoO at about 1178K in air, however, there were no CoO peaks found in patterns at 1213K and 1273K.

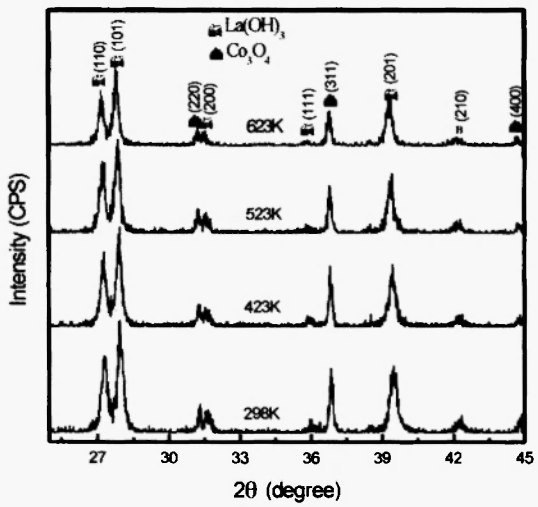

(a) at 298K, 423K, 523K and 623K

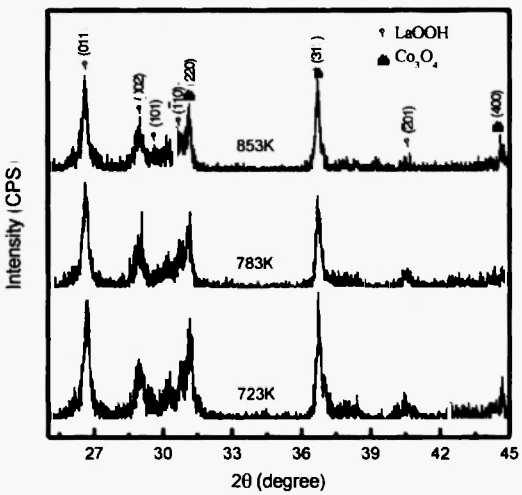

(b) at 723K, 783K and 853K

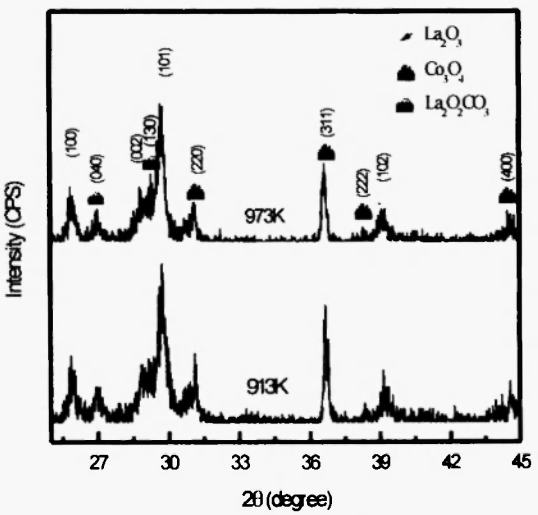

(c) at 913K and 973K

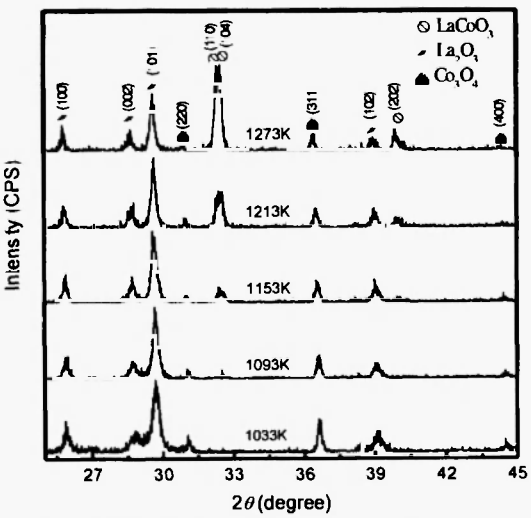

(d) at 1033K, 1093K, 1153K, 1213K and 1273K

Fig. 1: High temperature XRD patterns of La_2O_3 and Co_3O_4 powder mixture

3.2 TG-DSC measurements

Fig. 2 (a)-(c) are TG-DSC curves with heating rates of 0.1667K/s (10K/min), 0.3333K/s (20K/min) and 0.5K/s (30K/min) respectively. The figures show a slight weight loss and a small endothermic effect below 573K, which could be due to the desorption of physically adsorbed moisture.

Fig. 2 (a)-(c) demonstrates four weight losses, accompanied by three sharp endothermic peaks from 573K to 1173K. The first weight loss may occur from 573K to 673K accompanied by a sharp endothermic peak at about 623K. The relative weight losses with different heating rates were 7.2% (0.1667K/s), 8.0%(0.3333K/s) and 6.2%(0.5K/s), close to the theoretical weight loss 6.66 % if $La(OH)_3$ decomposes into LaOOH. In the high temperature X-ray diffraction measurements, $La(OH)_3$ decomposition took place in the range from 623K to 723K. So the weight loss at this stage may correlate to the $La(OH)_3$ decomposition into LaOOH.

Figs. 2(a)-(c) illustrate the weight loss from 673K to 873K and an endothermic peak at about 773K. The relative weight losses with different heating rates were 2.95% (0.1667K/s), 6.17 % (0.3333K/s) and 2.9% (0.5K/s) respectively.

From 873K to 1073K, the relative weight losses were 1.17% (0.1667K/s), 1.03% (0.3333K/s) and 0.8% (0.5K/s) respectively, and without significant endothermic peak.

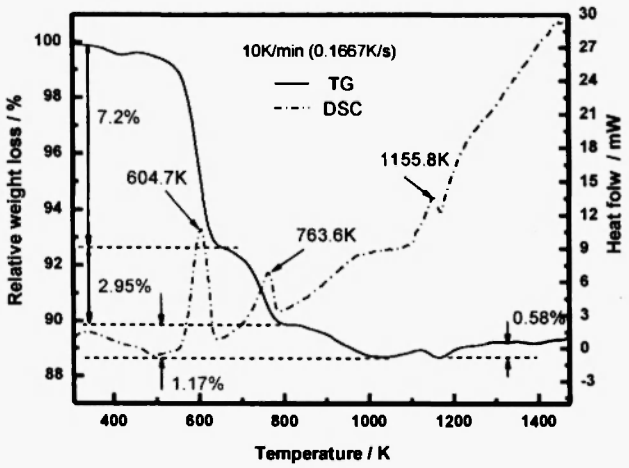

(a) heating rate: 0.1667K/s (10K/min)

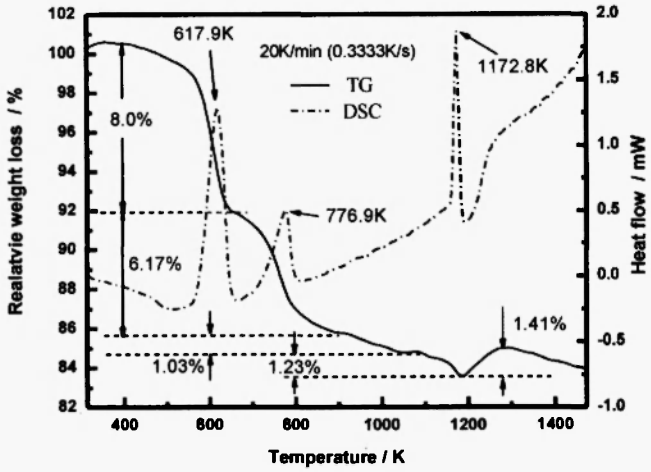

(b) heating rate: 0.3333K/s (20K/min)

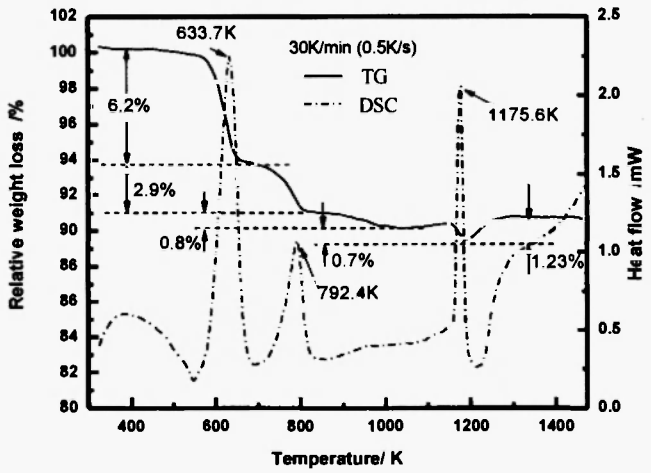

(c) heating rate: 0.5K/s (30K/min)

Fig. 2: TG–DSC curves of La_2O_3 and Co_3O_4 powder mixture

The total relative weight losses from 673K to 1073K were 4.12% (0.1667K/s), 7.2% (0.3333K/s) and 3.7% (0.5K/s). At 0.1667K/s and 0.5K/s, the data agree well with the theoretical weight loss 3.33% for all the LaOOH decomposing into La_2O_3. Comparing with the XRD patterns in Fig. 1(b) and (c), the weight loss from 673K to 873K could be caused by overlapping of LaOOH decomposion and $La_2O_2CO_3$ formation. The weight loss from 873K to 1073K could be due to $La_2O_2CO_3$ decomposition.

The weight losses around 1173K were 1.23%(0.3333K/s) and 0.7% (0.5K/s) respectively. It is known from the thermodynamic calculation that Co_3O_4

is converted into CoO at about 1178K in air, and the resultant theoretical weight loss is 1.97 %. Clearly, the above mentioned weight loss data were much less than theoretical value for Co_3O_4 decomposition. As can be seen in Fig. 1(d), weak peaks for $LaCoO_{3-\delta}$ in the XRD pattern have existed at 1093K. This may imply that $LaCoO_{3-\delta}$ could appear before Co_3O_4 decomposition started. The already formed $LaCoO_{3-\delta}$ layer may cover on the surface of Co_3O_4 particles, and in some extent, prevent the outward diffusion of the released O_2 by decomposition, therefore rising local partial oxygen pressure and preventing the further decomposition of Co_3O_4. This may be the reason why peaks of CoO can hardly be observed in the X-ray diffraction patterns of 1213K and 1273K in Fig. 1 (d).

The weight gain between 1173K and 1273K may correlate to the reaction between La_2O_3 and Co_3O_4 as:

$$3La_2O_3 + 2Co_3O_4 + (1/2-3\delta)\,O_2 = 6LaCoO_{3-\delta} \qquad (1)$$

It is noted that the reaction mechanism of converting La_2O_3 and Co_3O_4 powder mixture to $LaCoO_{3-\delta}$ can be clarified by the combination of high temperature X-ray diffraction and TG-DSC measurements.

3.3 $LaCoO_{3-\delta}$ preparation using tablets at isothermal heating conditions

As mentioned earlier, using room temperature XRD measurements with the matrix-flushing approach proposed by Chung /22/, the fractional conversion to $LaCoO_{3-\delta}$ in a tablet quenched after heating can be determined. Fig. 3 is a typical X-ray diffraction pattern of a composite sample with 2θ scanning from 10°-90°. It can be seen that (110) and (104) peaks for $LaCoO_{3-\delta}$ and (111) peak for Ag do not overlap with that of other compounds. The three selected peaks are completely within the 2θ scanning range from 30° to 40° for all the composite samples. Figs. 4 (a) through (f) demonstrate the XRD patterns for the composite samples corresponding to the heat treatment temperatures 983K, 1043K, 1103K, 1133K, 1163K and 1223K respectively. Using the treatment by Chung, the relative intensity of the selected peaks to that of Ag can be used to evaluate the mass fraction of $LaCoO_{3-\delta}$ in composite samples, and then the fractional conversions. In order to reduce the experimental deviations, three room XRD measurements were taken for each heating time at a specified temperature. The arithmetic means of the three fractional conversion values are summarized in Table 2.

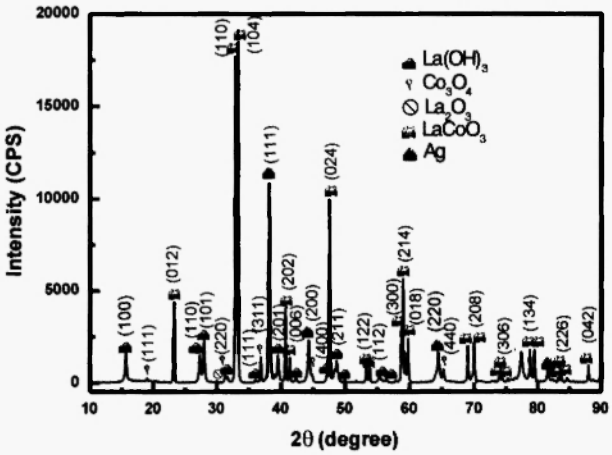

Fig. 3: X-ray diffraction pattern of composite sample

In solid-state reactions, the formation process of solid product often involves several steps: the nuclear formation and growth, the movement of phase (reacting interface) boundary and the diffusion of reactant species through the product layer. The kinetic equations regarding the various rate-controlling steps have been well established. The cases of rate controlling by nuclear formation and growth, or by the movement of phase (reacting) boundary often occur at the initial stage, and at relatively lower temperature. At higher temperature, diffusion usually is the rate-controlling step due to its slower rate. In the present study, three-dimension diffusion models by Ginstling- Brounshtein /23/, Jander /24/, and Dunwald-Wagner /25/ equations have shown much better fittings among others.

Dunwald-Wagner equation derived for solid-state reactions from Fick's second law can be expressed as:

$$\alpha = 1 - \frac{6}{\pi^2}\sum_{n=1}^{\infty}\frac{1}{n^2}\cdot e^{-\frac{n^2\pi^2 D\cdot t}{r_0^2}} \qquad (2)$$

where α is the fraction of conversion, t is diffusion time, D denotes the diffusion coefficient and r_0 is the radius of the sphere particle. The second term on the right hand side in Eq. 2 is an infinite series. In the present

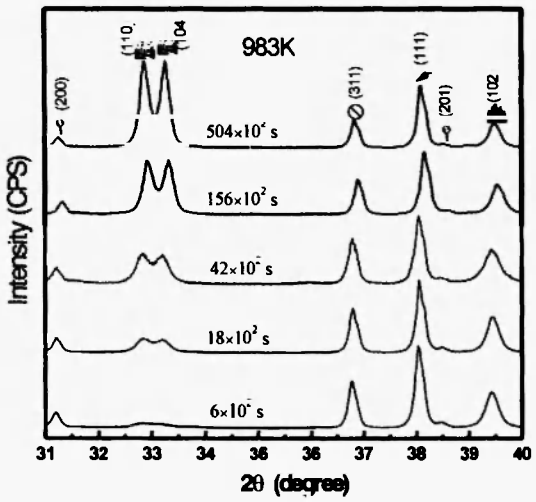

(a) 983K

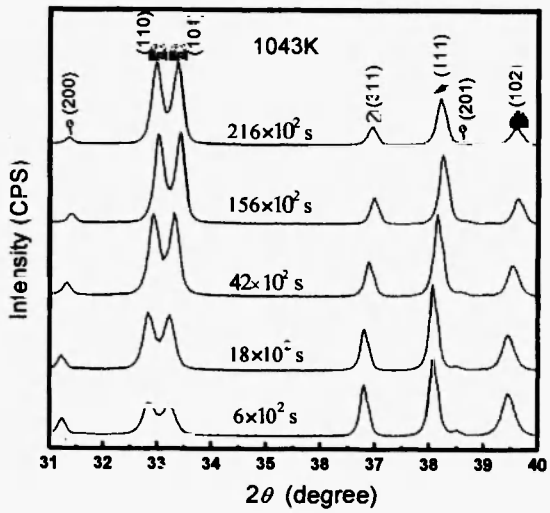

(b) 1043K

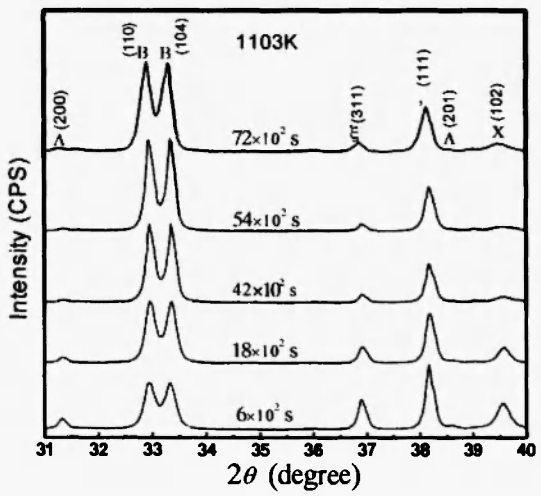

(c) 1103K

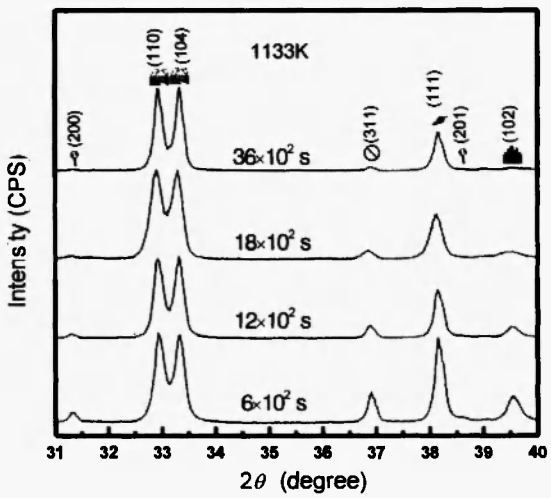

(d) 1133K

continued...

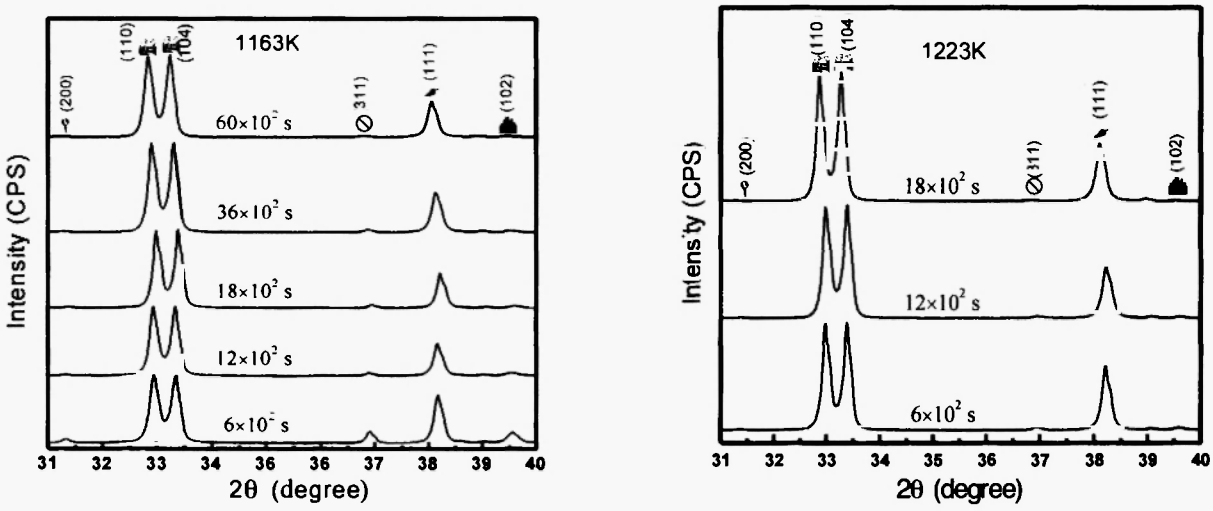

(e) **1163K** (f) **1223K**

Fig. 4: Part (31° - 40°) of diffraction patterns for composite samples

♦ – $La(OH)_3$ ▼ – $LaCoO_3$ ★ – Co_3O_4 ● – Ag ▽ – La_2O_3

Table 2

Relationship between fractional conversion (α) and time at various experimental temperatures

Time / 10^2 s	Fractional conversion					
	983K	1043K	1103K	1133K	1163K	1223K
6	0.0338	0.1824	0.3143	0.4594	0.5831	0.7533
12	0.0650	0.2268	0.4131	0.6964	0.8285	0.9224
18	0.0923	0.2738	0.5326	0.7767	0.8925	0.9453
30	0.1526	0.3536	0.6609	0.8527	—	—
36	—	—	—	—	0.9534	—
42	0.1953	0.4273	0.7617	—	—	—
54	0.2359	0.4526	0.8019	—	—	—
60	—	—	—	—	0.9798	—
72	0.2478	0.5236	0.8540	—	—	—
156	0.3654	0.6361	—	—	—	—
216	0.4015	0.7204	—	—	—	—
504	0.5277	—	—	—	—	—

treatment, n =10 was taken. In this way, the deviation between the limit of sum of the infinite terms and the sum of the finite (10) terms could be enough smaller than the experimental error for α. Fig. 5(a) and (b) demonstrate the Dunwald-Wagner fittings, where (a) corresponds to 983K and 1043K, (b) to the four remaining higher temperatures.

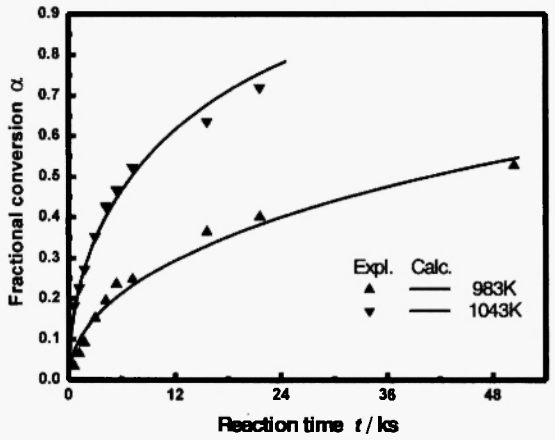

(a) 983K and 1043K

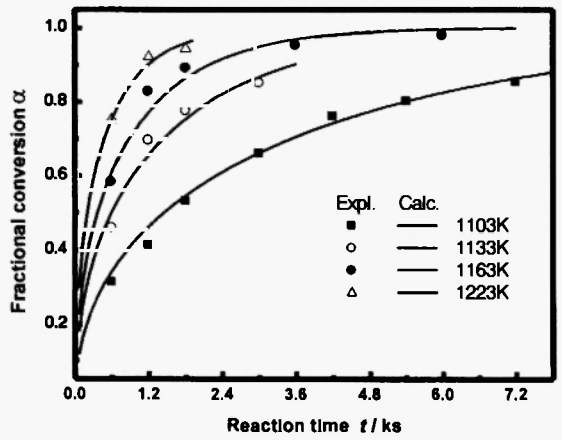

(b) 1103K, 1133K, 1163K, 1223K

Fig.5: Relationship between fractional conversion and time at 983K, 1043K, 1103K, 1133K, 1163K and 1223K. Marks are experiment data. Solid lines are calculated using Eq. 2

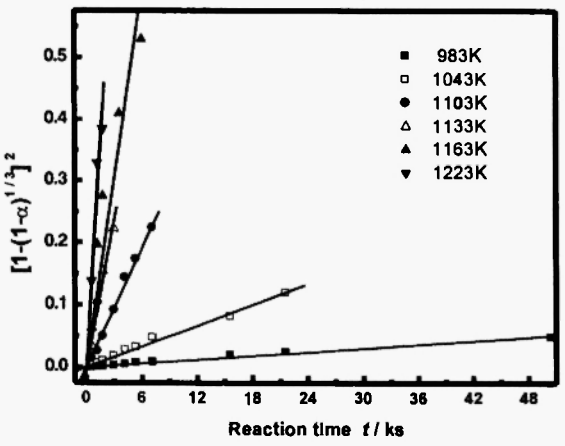

Fig. 6: The fitting of experimental fractional conversion with time using Jander's equation

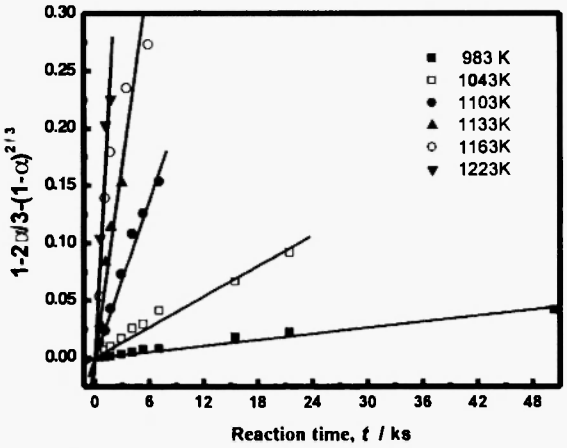

Fig. 7: The fitting of experimental fractional conversion with time using Ginstling-Brounshtei equation

Figs. 6 and 7 are similar figures showing respectively the fittings using Jander and Ginstling-Brounshtein equations at various temperatures.

From Figs. 5-7, it can be observed that the precisions of the three fittings are commonly good. However Dunwald-Wagner and Jander equations may follow the reaction better than Ginstling-Brounshtein model. The linear Jander-fittings have generated larger correlated coefficients and small standard deviations than those for the relevant Ginstling-Brounshtein fittings at every experimental temperature. The precisions obtained in the two linear fittings at 1163K seem not as good as those for other experimental temperatures. Such a fact has not been found from Fig. 5(b) for Dunwald-Wagner's fitting. The reason needs further investigatation.

The above analysis indicates that three-dimensional diffusion through product layer was likely to be the rate-controlling step during the overall reaction process.

3.4 Apparent activation energy

The D/r_0^2 in Dunwald-Wagner's equation and the rate constant k in Jander's equation at different experimental temperatures are shown in Table 3.

Arrhenius plots using apparent rate constants (k) from Jander fittings and D/r_0^2 from Dunwald-Wagner's fitting are shown in Fig. 8 and Fig. 9, and yield apparent activation energies of 235.4 and 231.8 kJ/mol respectively. These two values agree well with

each other, the mean is 233.6 kJ/mol.

Table 3
Apparent rate constants at various experimental temperatures

Temperature / K	Dunwald-Wagner equation $\frac{D}{r_0^2}$ / s^{-1}	Jander equation k / s^{-1}
983	$0.075^{5}10'$	$0.100^{5}10'$
1043	$0.432^{5}10'$	$0.550^{5}10'$
1103	$2.123^{5}10'$	$3.167^{5}10'$
1133	$5.177^{5}10'$	$7.800^{5}10'$
1163	$8.432^{5}10'$	$10.050^{5}10'$
1223	$15.470^{5}10'$	$23.233^{5}10'$

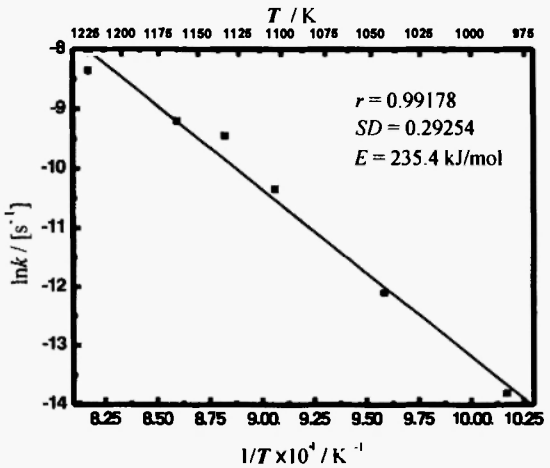

Fig. 8: Temperature dependence of k obtained from Jander fittings

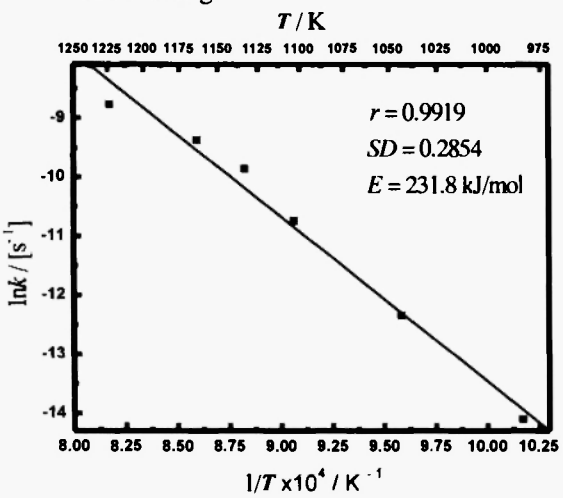

Fig. 9: Temperature dependence of D/r_0^2 obtained from Dunwald-Wagner fittings

4 DISCUSSION

It is not possible to determine the non-stoichiometry for oxygen in lanthanum cobaltate from its XRD patterns right now. However, it is known that the product compound obtained in the present study was oxygen deficient /1,20/. The oxygen deficiency δ can be roughly estimated from present experimental temperature and atmosphere, as much as 0.0003 at 1226K.

In spite of the chemical changes: $La(OH)_3 \rightarrow LaOOH$, $LaOOH \rightarrow La_2O_3$, $LaOOH \rightarrow La_2O_2CO_3$, $La_2O_2CO_3 \rightarrow La_2O_3$ below 973K, at higher temperature (>973K) oxygen as gaseous species also participated in the reaction indicated in Eq. (1). Clearly, oxygen diffusion through the boundary layer of the gas phase around particles may not be the rate-controlling step. In the experiments, 0.6g La_2O_3 and Co_3O_4 powder mixture was pressed into a tablet of ϕ 12mm×1.7mm, the porosity can be calculated as much as 0.5838. From the density data of 7290, 6574 and 6056 kg/m^3 for $LaCoO_3$, La_2O_3 and Co_3O_4, it is known that the volume ratio of the product to the reactants for the reaction shown in Eq. 1 could be 0. 88. This means that the $LaCoO_{3-\delta}$ product layer formed on the particle surface could be looser. The larger porosity of the sample and the looser product layer may have resulted a faster oxygen diffusion within the solid product layer. In Fig. 4 (a)-(f), a weak (200) $La(OH)_3$ peak can been observed showing that $La_2O_2CO_3$ and amount of $La(OH)_3$ have been converted to La_2O_3 during the temperature rising and the first 10 minute iso-thermal heating. The remaining small amount of $La(OH)_3$ continued to decompose, converting into La_2O_3 and released water. However this gas/solid reaction has been noted not rate-predominant. The experimental results described in subsection 3.3 have shown that the overall process of $LaCoO_{3-\delta}$ synthesis under iso-thermal calcinations using tablet samples could be controlled by diffusion of solid ionic species.

The concern is which kind of solid-state ions, La^{3+}, Co^{3+} or O^{2-}, diffuse across the product layer with the lowest rate among others. We shall try to make such an estimation using the knowledge from the defect structure of $LaCoO_{3-\delta}$ and tracer diffusion coefficient of oxygen ions in $LaCoO_{3-\delta}$ single crystal.

Seppänen *et al.* /1/ determined the ionic defect structure of single-phase $LaCoO_{3-\delta}$ as well as $LaCoO_{3-\delta}$ in equilibrium with CoO and La_2O_3 using solid electrolyte emf cell between 1178K and1311K. They proposed that oxygen vacancies were the major ionic defects.

Ishigaki *et al.* /2/ measured the tracer diffusion coefficient for oxygen ions, D_O^*, in $LaCoO_{3-\delta}$ single crystal in temperature range from 973K to 1273K by a gas-solid isotopic exchange technique using ^{18}O tracer. The temperature dependence of D_O^* in $LaCoO_{3-\delta}$ single crystal can be expressed as

$$D_O^*(cm^2 \cdot sec^{-1}) = 3.63\times10^4 e^{-\frac{309.6\pm20.9 kJ\ mole^{-1}}{RT}}$$

The diffusion coefficients obtained using Dunwald-Wagner's fitting in the present work and the tracer diffusion coefficients of oxygen ions in $LaCoO_{3-\delta}$ single crystal calculated using the equation derived by Ishigaki are listed in Table 4. It is seen that the diffusion coefficients obtained in the present work are as much as about two orders less than the tracer diffusion coefficients of O^- in $LaCoO_{3-\delta}$ single crystal. It can be estimated that the mobility of solid oxygen ions in $LaCoO_{3-\delta}$ layer in the tablet samples during the heating treatment should have been higher than that in $LaCoO_{3-\delta}$ crystal, for the higher defect densities in the former. So, the smaller diffusion coefficients listed in the right column of Table 4 may not correspond to the diffusion of O^- ions. In other words, the diffusion of oxygen ions in $LaCoO_{3-\delta}$ product layer cannot be the rate-controlling step.

Table 4

Trace diffusion coefficients of oxide ions in single crystal $LaCoO_{3-\delta}$ and diffusion coefficients obtained from Dunwald-Wagner model at various experimental temperatures

Temperature/ K	D_O^* /$m^2 \cdot s^{-1}$ obtained in $LaCoO_3$ single crystal	D/$m^2 \cdot s^{-1}$ using Dunwald-Wagner equation
983	0.013×10^{-14}	0.019×10^{-16}
1043	0.113×10^{-14}	0.111×10^{-16}
1103	0.789×10^{-14}	0.545×10^{-16}
1133	1.928×10^{-14}	1.330×10^{-16}
1163	4.502×10^{-14}	2.166×10^{-16}
1223	21.660×10^{-14}	3.975×10^{-16}

In the following statements, we need to explain which kind of cations, La or Co, diffusing more slowly and controlling the solid-state reaction. O'Connell and co-works /12/ have prepared pure $LaCoO_{3-\delta}$ perovskite with a bulk La/Co molar ratio of 1:1.1 by gel-type precipitation. PXRD, Rietveld analysis and density measurements showed that the perovskite was non-stoichiometric with a deficiency of lanthanum ions in the lattice. The cation vacancies were compensated by the presence of either higher valent cobalt or oxygen. The results of PXRD, Rietveld analysis and density measurements revealed that at La/Co molar ratio of 1:1, $LaCoO_{3-\delta}$ perovskite and lanthana were produced, and there were again lanthanum ions deficient in the structure of perovskite, however there the vacancies were compensated by the presence of anion vacancies.

In the present study, we also noted that with La:Co molar ratio of 1:1, it was hard to get pure $LaCoO_{3-\delta}$ perovskite, as there was some lanthana that remained, while it was easy to get a pure $LaCoO_{3-\delta}$ perovskite with La: Co molar ratio of 1:1.03. So our experimental fact also has supported the viewpoint that lanthanum ions vacancies exist in $LaCoO_{3-\delta}$.

Regarding the diffusion of cobalt ions, it is necessary to note the location of these ions in the lattice of $LaCoO_{3-\delta}$ perovskite. It is known that cobalt ions are located in octahedron of oxygen ions, which may limit their mobility. Also, lanthanum vacancies can result in higher valent cobalt, so the movement of cobalt ions is not easier.

From the above analyses, it could be estimated that the diffusion of lanthanum ions in $LaCoO_{3-\delta}$ product layer may most likely be the rate-controlling step in the overall reaction during the isothermal synthesis using tablets samples.

5. CONCLUSION

Using high temperature XRD measurements with TG-DSC technique, it has been estimated that the formation of $LaCoO_{3-\delta}$ with La_2O_3 and Co_3O_4 powder as raw materials (To the measurements, $La(OH)_3$ and Co_3O_4 mixture, instead, could be more precise.) has a complex mechanism, and consists of several steps.

(1) $La(OH)_3$ and Co_3O_4 were heated up, while there

were no chemical reactions observed below 623K.

(2) $La(OH)_3$ decomposition into LaOOH could be found within 623K and 723K.

(3) LaOOH decomposed into La_2O_3 within 853K and 913K, and the some amount of produced La_2O_3 simultaneously reacted with CO_2 in air, forming some $La_2O_2CO_3$.

(4) $La_2O_2CO_3$ decomposed into La_2O_3 within 973K –1033K. Only peaks of La_2O_3 and Co_3O_4 could be found in X-ray diffraction patterns at 1033K.

(5) In TG-DSC measurements, the weight loss around 1173K could be due to the partial decomposition of Co_3O_4. Thin $LaCoO_{3-\delta}$ layer formed before decomposition of Co_3O_4 may have prevented its further decomposition, so no peaks of CoO have been found in XRD patterns at 1213K and 1273K.

Regarding the kinetics and mechanism of $LaCoO_{3-\delta}$ synthesis from compacts of La_2O_3 and Co_3O_4 powder mixture under isothermal calcinations, the following information has been attained.

(1) No intermediate product between La_2O_3 and Co_3O_4 was found in the process.

(2) Dunwald-Wagner and Jander equations could be employed to describe the overall process satisfactorily. The relevant apparent activation energy values are 231.8 kJ/mol and 235.4 kJ/mol respectively.

(3) The overall reaction process could be controlled by diffusion of solid-state ions. The diffusion of lanthanum ions through the product $LaCoO_{3-\delta}$ layer could be the rate-controlling step.

ACKNOWLEDGEMENT

The financial support for the project 50374008 from National Science Foundation of China is gratefully acknowledged.

REFERENCES

1. M. Seppänen, M. Kyto, and P. Taskine, *Scand. J. Metall.*, **9**, 3-11 (1980).
2. T. Ishigaki, S. Yamauchi, J. Mizusaki et al., *J. Solid State Chem.*, **54**, 100-107 (1984).
3. G. Thornton, B. C. Tofiel and A. W. Hewat, *J. Solid State Chem.* **61**, 301-307 (1986).
4. O. Parkash, R. Kumar, D. Kumar, *J. Mater. Sci. Lett.*, 7, 383-385 (1988).
5. Y. Teraoka, H.M. Zhang, K. Okamoto et al., *Mater.Res.Bull.*, **23**, 51-58 (1988).
6. J. Mizusaki, I. Tabuchi, T. Matsuura, S. Yamauchi and K. Fueki, *J. Electrochem. Soc.*, **136**, 2082-2088 (1989)
7. L. W. Tai, M. M. Nasraliah, H. U. Anderson, D.M. Sparlin and S. R. Sehlin, *Solid State Ionics*, **76**, 259-271 (1995).
8. J. W. Stevenson, T. R. Armstrong, R. D. Carneim et al., *J. Electrochem, Soc.*, **143**, 2722-2729 (1996).
9. F. M. Figueiredo, J. A. Labrincha, J. R. Frade,et al., *Solid State Ionics*, **101-103**, 343-349 (1997).
10. K. Huang, H. Y. Lee and J. B. Goodenough, *J. Electrochem. Soc.*, **145**, 3220-3227 (1998).
11. W. Yang and Z. Sui, *Chinese J. Mater. Research*, **12**, 149-153 (1998).
12. M. O'Connell, A. K. Norman, C. F. Hüttermann and M. A. Morris, *Catalysis Today*, **47**, 123-132 (1999).
13. S. Li, W. Jin, N. Xu *et al.*, $O_{0.2}Fe_{0.8}O_{3-\delta}$ membrances. *Solid State Ionics*, **124**, 161-170 (1999).
14. S. Chaudhary, V. S. Kumar, S. B. Roy, et al., *J. Magn. Magn. Mater.*, **202**, 47-52 (1999).
15. S. Li, W. Jin and N. Xu., *J. Mater. Sci.*, **35**, 4329-4335 (2000).
16. W. Ma and G. Xie, *Trans. Nonf. Met. Soc. China*, **11**, 904-907 (2001).
17. S. Wang, M. Katsuki, M. Dokiya and T. Hashimoto, *Solid State Ionics*, **159**, 71-78 (2003).
18. L. Qiu, T. Ichikawa, A. Hirano, N. Imanishi and Y. Takeda, *Solid State Ionics*, **158**, 55-65 (2003).
19. S. Nakayama, O. Kazaki, Y. L. Aung and M. Sakamoto, *Solid State Ionics*, **158**, 133-139 (2003).
20. J. Mizusaki, Y. Mima, S. Yamauchi et al, *J. Solid State Chem.* **80**, 102-111 (1989).
21. B. J. Yan, J. Y. Zhang and J. H. Liu, *J. Rare Earths*, unpublished work (2004).
22. B. F. Chung, *J. Appl. Cryst.*, 7, 519-525 (1974).
23. A. M. Ginstling and, B. I. Brounshtein, *J. Appl. Chem., USSR*, (English translation), **23**, 1249-1259 (1950).
24. W. Jander, *Z. Anorg. Allg. Chem.*, **163**, 1-30

(1927).

25. H. Dunwald and C. Wagner, *Z. Phys. Chem* , **B24**, 53 (1934).
26. F. M. Figueiredo, M. Jafelicci Jr., C.O. Paiva-Santos, et. al., *J. Magn. Magn. Mater.*, **226** (Suppl. 1), 812-814 (2001).
27. H. P. He, X. J. Huang and L. Q. Chen, *J. Phys. Chem. Solids*, **62**,701-709 (2001).
28. Z. G. Liu, L. G. Cong, X. Q. Chen, et. al., *J. Alloys Compds.*, **314**, 281-285 (2001).
29. W. Boujelben et. al., *Phys. Status Solid. (A) Applied Research*, **191**, 243-254 (2002).
30. X. Q. Huang, L. Pei, Z. G. Liu *et. al.*, *J. Alloys Compds.*, **345**, 265-270 (2002).